

# Magnetic resonance imaging at microscopic resolution reveals subtle morphological changes in a mouse model of dopaminergic hyperfunction

Michel Cyr,<sup>a</sup> Marc G. Caron,<sup>a,\*</sup> G. Allan Johnson,<sup>b</sup> and Aki Laakso<sup>a</sup>

<sup>a</sup>Department of Cell Biology, Center for Models of Human Disease, IGSP, Box 3287, Duke University Medical Center, Durham, NC 27710, USA

<sup>b</sup>Center for In Vivo Microscopy, Box 3302, Duke University, Durham, NC 27710, USA

Received 5 July 2004; revised 24 November 2004; accepted 7 January 2005  
Available online 9 March 2005

Structural abnormalities of the basal ganglia have been documented in several neuropsychiatric conditions associated with dysregulation of the dopamine system. However, the histological nature underlying these changes is largely unknown. Using magnetic resonance imaging at microscopic resolution (MRI, 9.4 T with 43  $\mu\text{m}$  isotropic spatial resolution) and stereological techniques, we have investigated the effect of increased dopamine neurotransmission on brain morphology in mice with elevated extracellular dopamine, the dopamine transporter knockout (DAT-KO) mice. We first demonstrate the usefulness of MRI at microscopic resolution for the accurate identification and measurement of volumes of specific subregions, accounting for less than 0.03% (0.16  $\text{mm}^3$ ) of the volume of a mouse brain. Furthermore, the MRI analysis reveals a significantly lower volume (–9%) of the anterior striatum of DAT-KO mice, while the volume of other dopamine-related structures such as the posterior striatum and the substantia nigra pars reticulata is unchanged in comparison to wild type littermates. Stereological analysis performed in the same brains reveals that one important structural factor accounting for this selective change in volume is a reduction of 18% in the absolute number of neuronal cell bodies. The feasibility of assessing accurately small morphological alterations in mouse models, where the molecular and histological pathologies can be easily compared in a controlled manner, provides a paradigm to examine the relevance of selective brain volumetric changes associated with a number of neuropathological conditions.

© 2005 Elsevier Inc. All rights reserved.

**Keywords:** MRI; Neuropsychiatric disorders; Basal ganglia; Dopamine transporter; Brain morphology; Mouse models

---

## Introduction

Dopamine (DA) is a major neuromodulator in the brain and dysfunction in DA neurotransmission has been associated with neuropsychiatric conditions such as schizophrenia, Tourette's syndrome, and attention deficit/hyperactivity disorder (ADHD)

(Abi-Dargham et al., 2000; Carlsson et al., 2000; Castellanos and Tannock, 2002; Hietala et al., 1995; Robertson and Stern, 1997; Swanson and Volkow, 2002; Tamminga and Carlsson, 2002). In order to better understand the neurological basis of these disorders, magnetic resonance imaging (MRI) analysis has been extensively performed in the brains of neuropsychiatric patients. However, even though several morphological changes have been documented, the clinical implications and significance of these findings remain contentious (Gogtay et al., 2002; Shenton et al., 2001). The current morphological approaches that include comparisons between in vivo imaging of human brains and histological studies of postmortem samples have been unsatisfactory because of the intrinsic disparity among populations such as age, gender, duration of illness, treatments, symptoms as well as number of recurrent episodes (Pakkenberg and Gundersen, 1997). In addition, whether the apparent dysfunction in DA neurotransmission associated with neuropsychiatric conditions contributes to the morphological changes observed by MRI cannot be easily established. Production of genetically altered mice provides a good implement to integrate symptoms or biochemical manifestations of human diseases with brain morphological, biochemical, and histological pathologies (Gainetdinov et al., 2001).

The challenges of mapping genotype to phenotype have generated an extraordinary range of approaches from gene chips to imaging. Each of the methodologies has its strengths and weaknesses. Integration of these approaches to draw meaningful conclusions requires an increasing diversity of expertise. Moreover, one common element to the majority of these methods is the volume of data generated. The work reported here makes use of the Mouse Bioinformatics Research Network (MBIRN) (<http://www.nbirn.net/TestBeds/Mouse/index.htm>), which has been established to help integrate these diverse disciplines and to make large volumes of data generated available to the neuroscience community.

A mouse model of increased DA neurotransmission has been generated by the inactivation of the dopamine transporter (DAT) gene and remarkable neurochemical and behavioral changes reflecting the enhanced activity of the DA system have been well documented in these mice (Cyr et al., 2003; Gainetdinov et al.,

---

\* Corresponding author.

E-mail address: caron002@mc.duke.edu (M.G. Caron).

Available online on ScienceDirect ([www.sciencedirect.com](http://www.sciencedirect.com)).

1999; Giros et al., 1996; Jones et al., 1998). As part of the MBIRN project, we have investigated the effect of increased dopamine neurotransmission on brain morphology by performing MRI at microscopic resolution (9.4 T with 43  $\mu\text{m}$  isotropic spatial resolution) in the DAT knockout (DAT-KO) mice. The use of MRI at microscopic resolution for studies of fixed tissues, where the confound of physiological motion can be eliminated and active stains can be used to augment differences between tissue structure, has been suggested before to obtain higher resolution (Johnson et al., 1993; 2002).

The present study demonstrates that MRI at microscopic resolution delineates with a high degree of confidence subtle morphological changes in the DAT-KO mouse brain. Moreover, by means of the ability to superimpose the MRI data with classical histological and immunofluorescence findings, we provide evidence that a selective decrease in the number of neuronal cell bodies in the anterior striatum, which would have otherwise been difficult to evaluate, presumably accounts for the structural changes.

## Methods

### Mice

Male DAT-KO ( $n = 4$ ) and WT mice ( $n = 4$ ) between 4 and 8 months of age were used in this study. The mice were housed in an animal care facility at 23°C on a 12-h light/12-h dark cycle with food and water provided ad libitum. Animal care was in accordance with the *Guide for Care and Use of Laboratory Animals* (NIH publication 865-23, Bethesda, MD) and approved by the Institutional Animal Care and Use Committee. Generation of DAT-KO C57BL/6J129SvJ mice was described previously (Giros et al., 1996) and the mice have been intercrossed for more than 10 generations.

### Tissue preparation

Mice were anesthetized with a combination of 3% isoflurane and an intraperitoneal injection of pentobarbital (50 mg/g body weight) and were transcardially perfused with 20 ml of 0.9% NaCl (37°C) followed by 100 ml of a cold (4°C) mixture 20:1 (by volume) of 10% buffered formalin and Prohance (Gadoteridol, Bracco Diagnostics, NJ). This tissue staining process results in reduction of the spin lattice relaxation time (T1) of all the tissues by more than 10 $\times$  in turn producing a roughly 8 $\times$  increase in the signal to noise ratio (Johnson et al., 2002). The mouse brain was removed and stored at 4°C in the same perfusion buffer overnight and scanned within 24 h. Before the high resolution scan is performed, an experienced technician adjusted the brain in its proper position by performing low resolution scans in order to get preliminary images of coronal sections. The correct coronal plane was determined by comparison with the coronal brain sections depicted in the mouse brain atlas of Paxinos and Franklin (2001). Once the imaging was acquired, the brains were immersed 10 s in isopentane (Sigma, MO) over dry ice and stored at  $-80^{\circ}\text{C}$  for histological studies. Adjacent coronal brain sections of 20  $\mu\text{m}$  were sliced using a cryostat (model HM500 OM, Microm) and kept in PBS solution at 4°C until used. To ensure that the coronal brain sections sliced by the cryostat were in the exact same coronal plane as the MRI images, we have compared the sections with the coronal MRI images and the coronal sections depicted in the mouse brain atlas of Paxinos and Franklin (2001)

and adjusted the correct position of the brain accordingly. Note that we used bregma, the point of junction of the coronal and sagittal sutures of the skull, as a standard for anatomical reference for distance (Paxinos and Franklin, 2001). For every brain structure analyzed by MRI and histology techniques, the registration of the location from bregma was determined as follows: the distance from bregma was attributed to the first section where the brain structure was distinguished, by comparison with the coronal sections depicted in the mouse brain atlas of Paxinos and Franklin (2001), and the subsequent adjacent sections of the structure were identified using their actual distance from the first section. For example, the first coronal MRI sections where the striatum was observed corresponded to +1.780 from bregma, the distance of 1.737, 1.694, 1.651, etc. (at a distance of 43 $\mu\text{m}$ ) were attributed to the following adjacent sections.

### MRI

All magnetic resonance imaging (MRI) was performed on a 9.4 T vertical bore Oxford magnet equipped with shielded gradients achieving peak strength of 850 mT/m. Images were acquired with 3 dimensional rf refocused spin warp encoding on 3 D ( $256 \times 256 \times 512$ ) image arrays covering an  $11 \times 11 \times 22$  mm field of view yielding isotropic voxels of  $43 \times 43 \times 43 \mu\text{m}$  ( $8 \times 10^{-5} \text{mm}^3$ ) T1 weighted images were acquired with TR = 100 ms, TE = 5 ms, NEX = 4. Perfusion with contrast agent reduces the mean T1 to <200 ms allowing acquisition of a T2 weighted image with a much shorter TR (200 ms) and TE (15 ms) than might be used with unstained (formalin fixed) tissues. NEX was reduced to 2. Both the T1 and T2 weighted image sets were acquired in 7.28 h.

### Histological assessment

All histological studies have been performed in the same brains used for MRI imaging. For Nissl staining, the sections were mounted on microscope slides (Superfrost™, Fisher Scientific). The slides were incubated 20 min at room temperature in a solution of 1% (wt/vol) Cresyl Fast Violet (Electron Microscopy Sciences, PA) in water containing 0.0025% (vol/vol) acetic acid and consecutively rinsed with 95% (wt/vol) ethanol, 100% (wt/vol) ethanol, 1:1 ethanol/xylene, and pure xylene for 1 min each at room temperature. Once sections were dried (few minutes), they were covered with a cover slip using D.P.X™ mounting medium (Electron Microscopy Sciences).

For immunofluorescence, free-floating sections were immunostained using the primary antiserum directed against the dopamine transporter (MAB369, Chemicon, CA), NeuN (MAB377, Chemicon), or GFAP (MAB360, Chemicon). Then, the sections were incubated with the appropriate labeled secondary antibody (Vector Laboratories, CA). The sections were also incubated 10 min at RT with a marker of cell nucleus, the Hoechst dye 33342 (Molecular Probes, OR), at a dilution of 1:10,000 in PBS. Sections were then slide-mounted using vectashield™ (Vector laboratories Inc., CA) and cover slipped.

### Volume determination

3 D MRI files with matrix dimensions =  $256 \times 256 \times 512$  were analyzed using Image J (<http://rsb.info.nih.gov/ij/>) and MRPath (Durham, NC) software with the observer blind to genotypes. The acquisition scheme described above provided

clear white/gray matter borders that were confirmed by association to histological analyses. The volume of the entire brain, the lateral ventricles, the striatum, the ventromedial nucleus of the hypothalamus, the ventrolateral geniculate nucleus, and the substantia nigra pars reticulata were measured by drawing the boundaries (segmentation) of each structure in the coronal plane on a section by section basis and summing all of the voxels contained in these structures. The borders of the brain, striatum, and lateral ventricles were drawn and checked in three orthogonal planes to ensure accuracy.

The volume of the striatum by histological analysis was evaluated according to the principle of Cavalieri (volume =  $s_1d_1 + s_2d_2 + \dots + s_nd_n$ , where  $s$  = surface area and  $d$  = distance between two sections). The Cavalieri principle is applied to histological data because of the limited number of sections selected. We considered 11 anatomical levels of the striatum for the volume estimation of every brain, which corresponded to one 20- $\mu\text{m}$  section every 200  $\mu\text{m}$  (+1.78 to -0.81 from bregma, Paxinos and Franklin, 2001). Image capturing was performed by using a light microscope (wild M3Z, Leica, 2.5 $\times$ ) coupled to a color digital camera (Spot RT, Diagnostic Instruments Inc). The surface area was calculated in each of the 11 Nissl-stained sections by contour drawing the striatum on each brain hemisphere using the IPLab software for Windows v3.0 (BioVision Technologies Inc). The value of surface area for one section was the number of pixels contained in the striatum  $\times$  138.4  $\mu\text{m}^2/\text{pixel}$ . Since images were scaled-up using a microscope (2.5 $\times$ ), the size of pixels has been determined using a microscale of 1  $\text{mm}^2$ . Data were expressed as the average Cavalieri volume ( $\text{mm}^3$ )  $\pm$ SEM of 4 mice per group.

#### Cell counts

Strict stereological methods have been performed for the assessment of the number of total striatal cells, neurons, and glial cells (Oorschot, 1996). Immunofluorescence studies were performed using Hoechst dye 33342, NeuN, and GFAP antibodies to label, respectively, striatal cell bodies, neurons, and glial cells. A Zeiss confocal microscope (LSM-510) was used for viewing of sections and capturing of images. Eight anatomical levels of the striatum were analyzed within the interval +1.61 to -1.35 from bregma (Paxinos and Franklin, 2001). Four sections have been considered for the anterior striatum (+1.78 to +0.50 from bregma; Paxinos and Franklin, 2001) as well as four sections for its posterior part (+0.49 to -2.21 from bregma; Paxinos and Franklin, 2001). Anatomical landmarks such as aspect, size, and situation of the anterior commissures, corpus callosum, septum, lateral ventricles, striatum, nucleus accumbens, and pallidum were used to ensure that levels studied were similar within and between groups. To determine the absolute total cell number, the average number of positive cells sampled on a limited volume was multiplied by the volume determined by MRI analysis for the anterior and posterior parts of striatum. The average number of cells per section was from eight 0.23  $\mu\text{m}^3$  (0.125  $\text{mm} \times 0.125 \text{mm} \times 15\mu\text{m}$ ) counting areas per hemispheres (40 $\times$  objective), four systematically placed in the dorsal part of the striatum and four in its ventral part. The final estimation of the cell numbers per animal was the average of positive neurons per  $\text{mm}^3$  sampled in both hemispheres of the section in 4 different sections as described above  $\pm$ SEM from 4 mice per group. All sections were coded and quantitative analyses of specimens were performed without the knowledge of genotypes.

#### Statistical analysis

Student's two-tailed  $t$  test was used for statistical comparisons between DAT-KO and wild type mice using GraphPad prism version 2.0 (Abacus concepts, Berkeley, CA).

## Results

#### MRI images

The present 9.4 T MRI acquisition protocol provides one of the highest resolutions of images with regard to contrast and clarity among discernible brain structures (Benveniste et al., 2000; Johnson et al., 2002; Redwine et al., 2003). Each image element (pixel) in a magnetic resonance image represents the signal from a volume (voxel) of tissue. One factor accounting for the high resolution of MRI images presented is the small size of voxels generated (7.9  $\times 10^{-5}$   $\text{mm}^3$ , 43  $\mu\text{m}$  along each axis). To give an order of magnitude, this voxel is almost equal to the size of a single Purkinje neuron in the mouse cerebellum (Sotelo, 1975). Another important factor is our method of fixation reported previously (Johnson et al., 2002). This method uses active stains that exploits the differences in tissue magnetization and provides high contrast between brain structures (Fig. 1). We use the term "active stain" as an analogy to more traditional stains used with conventional optical histology, e.g. the use of hematoxylin and eosin. In the context of this work, active stain refers to the perfusion method designed to reduce the T1 uniformly of all the tissues resulting in a 10 $\times$  increase in signal. The concentration has been chosen in such a fashion that many of the T2 differences in tissue are still evident but the uniform reduction in T1 allows scanning with much shorter repetition time (TR). The MRI files give three-dimensional images (matrix dimensions of 256  $\times$  256  $\times$  512) that can be viewed and sectioned in any plane (coronal, horizontal, and sagittal) without loss of spatial resolution (Fig. 1A, see Supplemental Data). The high resolution of the MRI images allows the distinction of several structures of the brain such as the olfactory tubercle, cerebral cortex, striatum, hippocampus, and cerebellum (Fig. 1B). Moreover, a number of dopamine-associated subregions, which make up brain structures, can also be identified from the MRI images such as, for example, the ventromedial nucleus of the hypothalamus (VMH), the ventrolateral geniculate nucleus (VLG), and the substantia nigra pars reticulata (SNr) (Figs. 1C–F).

One benefit of MRI is that the specimens are left intact for further analysis such as histological studies. In this way, several brain structures identified from the MRI images have been confirmed by histological analyses (Fig. 2A). For instance, the striatum, nucleus accumbens, and olfactory tubercle structures were identified by comparison with brain sections in which the dopamine nerve terminals were labeled using a DAT immunofluorescence as a marker (Fig. 2A, second panel).

#### Determination of volumes of brain structures

The segmentation, supported by histological analysis, was performed for the entire brain, the lateral ventricles, the striatum, the ventromedial nucleus of the hypothalamus, the ventrolateral geniculate nucleus, and the SNr by tracing contours of the border-zones of these structures in every MRI section (coronal, 43  $\mu\text{m}$

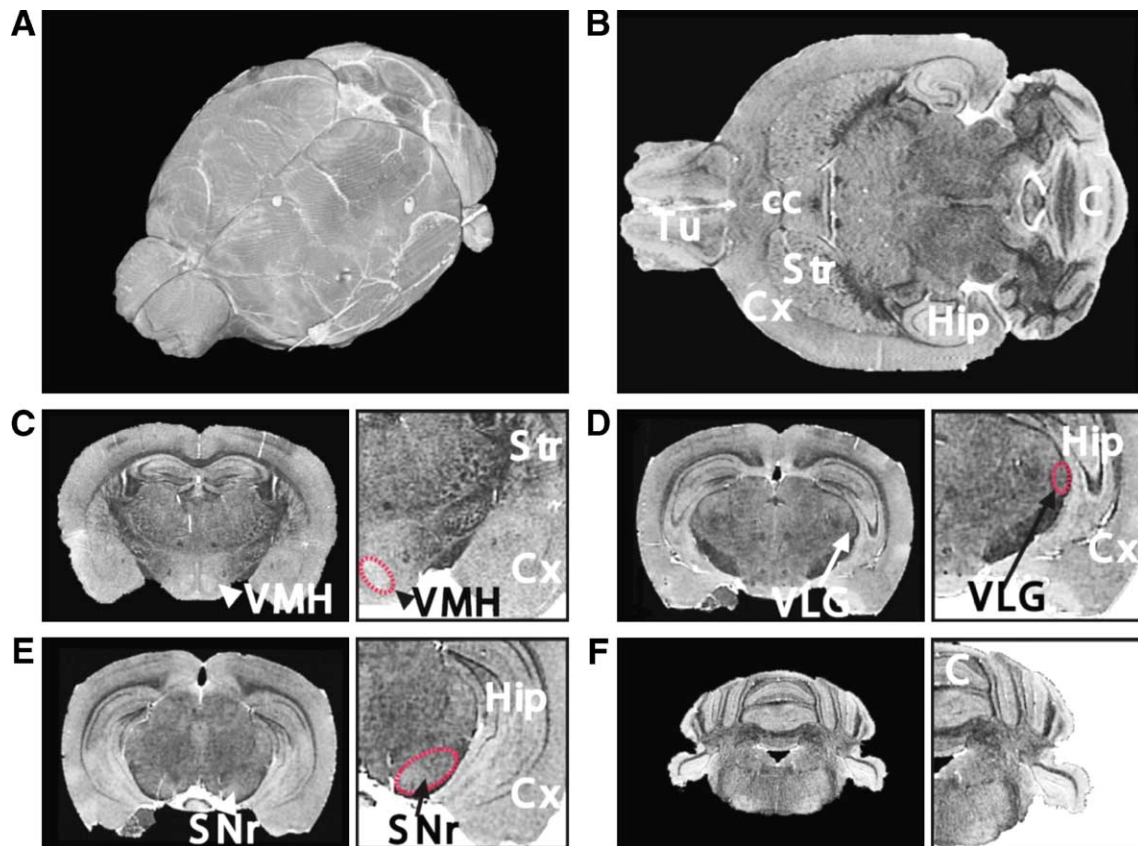


Fig. 1. Mouse brain structures visible with MRI at microscopic resolution. (A) Example of image acquired with three-dimensional radiofrequency refocused spin warp encoding on 3 D ( $256 \times 256 \times 512$ ) image arrays, covering an  $11 \times 11 \times 22$  mm field of view. (B) Example of a single horizontal section extracted from the high-resolution 3 D array. (C) Examples of coronal sections corresponding to bregma  $-1.58$  mm, (D) bregma  $-2.18$  mm, (E) bregma  $-3.28$  mm and (F), bregma  $-6.00$  mm (Paxinos and Franklin, 2001). C, cerebellum; cc, corpus callosum; Cx, cortex; Hip, hippocampus; Str, striatum; Tu, olfactory tubercle; VMH, ventromedial nucleus of the hypothalamus; VLG, ventrolateral geniculate nucleus; SNr, substantia nigra pars reticulata.

apart). The inter-rater reliability of the segmentation was very high since the variability between observers was 2.5% [ $r^2 = 0.9828$ ,  $P < 0.0001$ , Pearson's correlation analysis,  $n = 64$  segmentations (8 segmentations of striatum per mouse, 4 mice per group, two

observers)]. The manual segmentations were reconstructed (Fig. 2B) and the correctness of tracings in comparison with the border-zones of brain structures was verified in the coronal, sagittal, and horizontal plans.

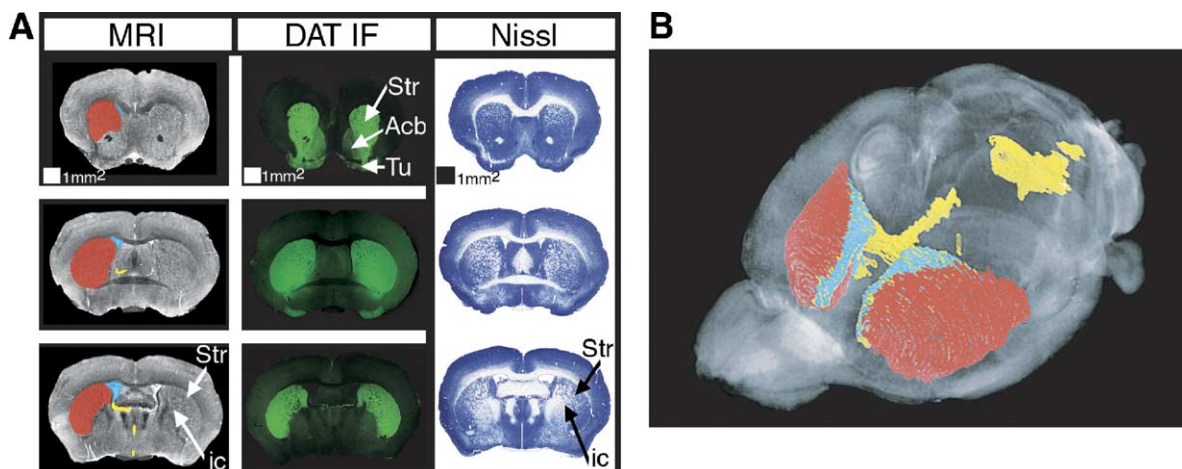


Fig. 2. Multimodal imaging of the mouse striatum structure and volume measurements. (A) Using the exact same brain, examples of coronal sections from MRI image acquisition, dopamine transporter immunofluorescence (DAT IF), and Nissl staining. The MRI and Nissl-stained sections correspond to bregma  $+1.18$  mm,  $+0.14$  mm, and  $-0.22$  mm in the first, second, and third panel respectively. The DAT IF correspond to bregma  $+1.16$  mm,  $+0.12$  mm, and  $-0.24$  mm in the first, second, and third panel respectively. Str, striatum; Acb, nucleus accumbens; ic, internal capsule and Tu, olfactory tubercle. (B) Example of 3 D image reconstruction from the contour-tracing of the striatum (red) as well as the lateral (blue), third, and fourth (yellow) ventricles.

The volumes were determined for every brain structure and no significant difference was observed between WT and DAT-KO mice in any of the brain regions and subregions in the initial analysis (Table 1). However, when the surface areas from each coronal section were plotted as a function of their distance from bregma, significantly lower surface areas of the striatum were found in sections of the DAT-KO compared to WT mice within the interval +1.78 to +0.50 mm from bregma (Paxinos and Franklin, 2001;  $P < 0.001$ , two-way repeated measures ANOVA comparing the profile curves; Fig. 3A). On the other hand, the striatal surface areas from the interval +0.49 to –2.21 mm from bregma (Paxinos and Franklin, 2001) as well as the surface areas of the lateral ventricles were not different (Fig. 3A). The length of the striatum was the same in both groups of mice (WT:  $3.99 \pm 0.06$  mm, DAT-KO:  $3.99 \pm 0.07$  mm,  $P = 0.95$  student's two-tailed  $t$  test). Based on these data, the striatum was divided in two parts, anterior, +1.78 to +0.50 mm from bregma and posterior, +0.49 to –2.21 mm from bregma (Paxinos and Franklin, 2001). Consequently, a significant decrease of 9% was observed in the volume of the anterior striatum of DAT-KO mice as compared to WT mice ( $P < 0.05$ , student's two-tailed  $t$  test) whereas the volume of the posterior striatum (Fig. 3B) was not statistically different ( $P = 0.79$ , student's two-tailed  $t$  test).

In addition to MRI measurement of volume, the same brains were also histologically prepared for stereological estimation of volume, using the Cavalieri principle (Oorschot, 1996). Within the interval +1.78 to –0.81 mm from bregma (Paxinos and Franklin, 2001), the striatal volumes from MRI analysis were comparable (WT:  $18.8 \pm 0.6$  mm<sup>3</sup>, DAT-KO:  $18.5 \pm 0.2$  mm<sup>3</sup>) to the striatal volumes estimated by histology using the Cavalieri principle (WT:  $18.5 \pm 0.8$  mm<sup>3</sup>, DAT-KO:  $18.2 \pm 0.3$  mm<sup>3</sup>). Furthermore, the total striatal volumes obtained by MRI analysis highly correlated with the volumes obtained by histology ( $r^2 = 0.92$ ,  $P = 0.0001$ ,  $n = 8$ , Pearson's correlation analysis). A previous report has also shown a close relationship between MRI measurements and histology (Cavalieri) volume estimations (Redwine et al., 2003).

#### Number of striatal cells and neurons

To investigate whether the morphological changes observed in DAT-KO mice could correlate with changes at the cellular level, further histological studies were performed in the very same brains used for MRI analysis. One factor that could influence changes in

volume is the number of glial cells. The glial cells of the striatum were labeled by immunofluorescence using an antibody against glial fibrillary acidic protein (GFAP; Fig. 4A). The disector method included the count of cells directly in a defined volume of tissue based on sampling schemes, counting rules, and disectors, which is a 3 D probe (Oorschot, 1996). Using this method, which takes into account the volume of the striatum of each mouse for every glial cell count, we observed a significant increase in the number of GFAP positive glial cells in the posterior striatum of DAT-KO as compared to WT mice, while no differences were noted in the anterior striatum (Fig. 4B). Another factor that could influence changes in striatal volume is neuronal density. Striatal neurons were identified by double labeling with Hoechst 33342 dye and the neuronal nuclei-specific protein (NeuN) antibody (Fig. 5A). Unbiased and systematic cell counts using the disector method (Oorschot, 1996) revealed a significantly lower number of neurons (–18%) in the anterior striatum of DAT-KO compared to WT mice (Fig. 5B). Interestingly, the total number of cells and neurons was similar in the posterior striatum between both genotypes (Fig. 5B). These stereological studies identified the lower number of neurons as an important factor that could underlie the reduction of volume in the anterior striatum of DAT-KO mice.

#### Discussion

We have demonstrated here the usefulness of using imaging methodologies, covering a range of scales from MRI at 43  $\mu$ m to <1  $\mu$ m levels using traditional histology, in delineating small morphological changes as well as to identify the underlying factors influencing brain volume in genetically altered mice, in this case the DAT-KO mice. The data will be made available to the neuroscience community via MBIRN as an “entry” in the mouse bioinformatics archives.

The high-resolution images paired with the non-destructive nature of MRI at microscopic resolution allowed accurate volume measurements. Here, we document for the first time that MRI provides the identification as well as the volume measurements of small subregions accounting for 0.03% ( $\sim 0.16$  mm<sup>3</sup>) of the volume of the mouse brain, which would otherwise be possible only using histological staining. Consequently, we document a selective and statistically significant decrease of 9% in the volume of the anterior striatum of the DAT-KO in comparison to WT mice, which previously failed to reach significance using histological techniques perhaps due to changes during tissue handling or storage (Fernagut et al., 2002, 2003). These findings reinforce the utility of the MRI approach for revealing small but meaningful pathological changes over more traditional techniques.

The combined MRI/stereological analysis not only established a highly sensitive detection of changes in the volume of the striatum of DAT-KO mice but also demonstrated the underlying factors that influence these changes, i.e., a decrease in the number of neuronal bodies. We found that neurons are the most affected population of cells since their absolute number is decreased by 18% while the absolute number of glial cell is unchanged in this region. Moreover, previous studies have shown that the striatal levels of well recognized markers of synaptic proteins, namely synapsin (a synaptic vesicle protein), syntaxin (a presynaptic plasma membrane protein), NF-H (neurofilament heavy chain subunit, an axonal marker), PSD-93 (postsynaptic density protein), SAP97 (synapse-associated protein 97), SAP102, and MAP-2

Table 1  
Volume measurements of different brain structures of wild type and DAT-KO mice by MRI at microscopic resolution

Structures	Corrected value (%)		P value
	Wild type	DAT-KO	
Brain	100	100	–
Lateral ventricles	$0.22 \pm 0.01$	$0.22 \pm 0.03$	0.87
Striatum	$4.50 \pm 0.10$	$4.35 \pm 0.09$	0.35
Substantia nigra pars reticulata	$0.27 \pm 0.02$	$0.28 \pm 0.01$	0.91
Ventrolateral geniculate nucleus	$0.042 \pm 0.002$	$0.055 \pm 0.005$	0.07
Ventromedial nucleus of the hyp.	$0.034 \pm 0.002$	$0.033 \pm 0.002$	0.89

Data are presented as the average corrected volume of the structure expressed in percentage ((volume of the striatum/volume of the brain)  $\times$  100) for every animal  $\pm$  SEM of 4 mice/group. The volume of the whole brain is  $470.9 \pm 16.3$  mm<sup>3</sup> for wild type and  $473.2 \pm 8.2$  mm<sup>3</sup> for DAT-KO mice.  $P$  values are based on a Student's two-tailed  $t$  test used for statistical comparisons between DAT-KO and wild type mice.

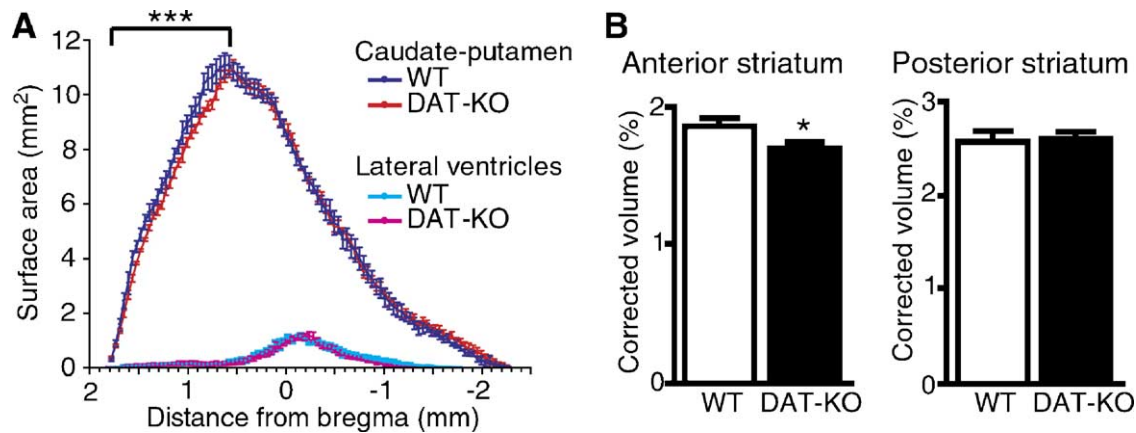


Fig. 3. Calculation of the volume of the striatum and lateral ventricles of mice by MRI at microscopic resolution. (A) The surface area for every matrix (each section =  $\sim 43 \mu\text{m}$ ) extracted from 3 D MRI files was measured by contour-tracing the entire striatum and lateral ventricles in wild type (WT) and dopamine transporter knockout (DAT-KO) mice. Data are the average surface area ( $\text{mm}^2$ )  $\pm$ SEM of 4 mice/group along the coronal axis of the brain.  $***P < 0.001$ ; WT vs. DAT-KO mice based on two-way repeated measures ANOVA comparing the profile curves. (B) Volume of the anterior (+1.61 to +0.50 from bregma; Paxinos and Franklin, 2001) and posterior (+0.49 to  $-1.35$  from bregma; Paxinos and Franklin, 2001) striatum normalized by the whole brain volume. Data are presented as the average corrected volume of the striatum expressed in percentage ((volume of the striatum/volume of the brain)  $\times 100$ ) for every animal  $\pm$ SEM of 4 mice/group.  $*P < 0.05$  WT vs. DAT-KO mice based on Student's two-tailed  $t$  test.

(microtubules-associated protein-2), were not different between WT and DAT-KO mice, suggesting that the pre- and postsynaptic structures are not significantly affected in DAT-KO mice (Yao et al., 2004). These findings are consistent with previous observations shown in the striatum of these mice of a lower number of GABAergic neurons expressing DARPP-32 and no changes in markers of nerve terminals such as DOPA decarboxylase and vesicular monoamine transporter levels (Cyr et al., 2003; Jaber et al., 1999; Jones et al., 1998).

Previous studies have shown that the persistent hyperdopaminergic tone observed in DAT-KO mice causes a pronounced locomotor hyperactivity and other aberrant behaviors (Cyr et al., 2003; Fernagut et al., 2003; Gainetdinov et al., 1999; Giros et al., 1996; Jones et al., 1998). We have documented recently that the excess of DA in the striatum of DAT-KO mice also causes the sporadic development of symptoms of motor dysfunction,

which were associated with apoptotic death of striatal neurons while the DA nerve terminals were spared (Cyr et al., 2003). Cell death is one possibility that could underlie a smaller striatal volume in these mice but a more complete study would be required since DA dysfunction can also affect brain structures through neurodevelopmental and remodeling mechanisms. However, these previous findings paired with the fact that the volume of the striatum is selectively affected in DAT-KO mice suggest that the 5-fold increase in extracellular DA found in the striatum of these mice is likely responsible for the structural changes (Cyr et al., 2003; Fernagut et al., 2003; Gainetdinov et al., 2001; Jones et al., 1998).

An increase in DA neurotransmission is a major biochemical manifestation documented in schizophrenia, Tourette's syndrome, and ADHD, and a small decrease in the volume of the caudate nucleus in these patients' brain is commonly observed by MRI

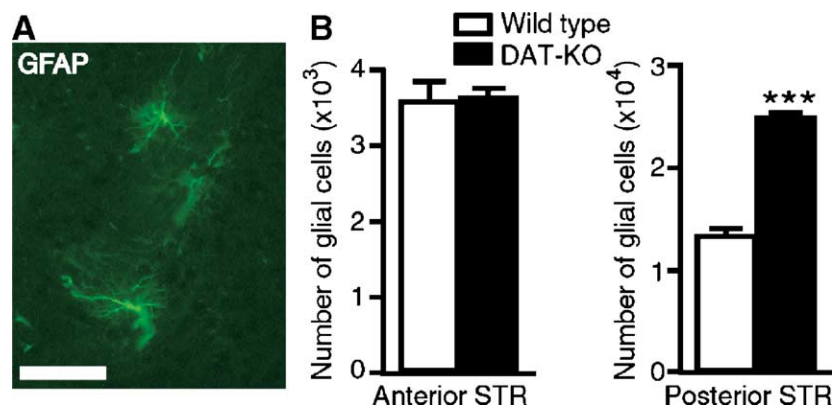


Fig. 4. Histological studies revealed the absolute number of glial cells. (A) Example of immunofluorescence staining in which glial cells are visualized using glial fibrillary acidic protein (GFAP) antibody. (B) The absolute number of glial cells was calculated by a strict stereological method in the anterior (+1.61 to +0.50 from bregma; Paxinos and Franklin, 2001) and posterior (+0.49 to  $-1.35$  from bregma; Paxinos and Franklin, 2001) striatum of wild type and dopamine transporter knockout (DAT-KO) mice. Data are the average glial cell counts  $\pm$ SEM of 4 mice/group.  $***P < 0.001$  WT vs. DAT-KO mice based on Student's two-tailed  $t$  test.

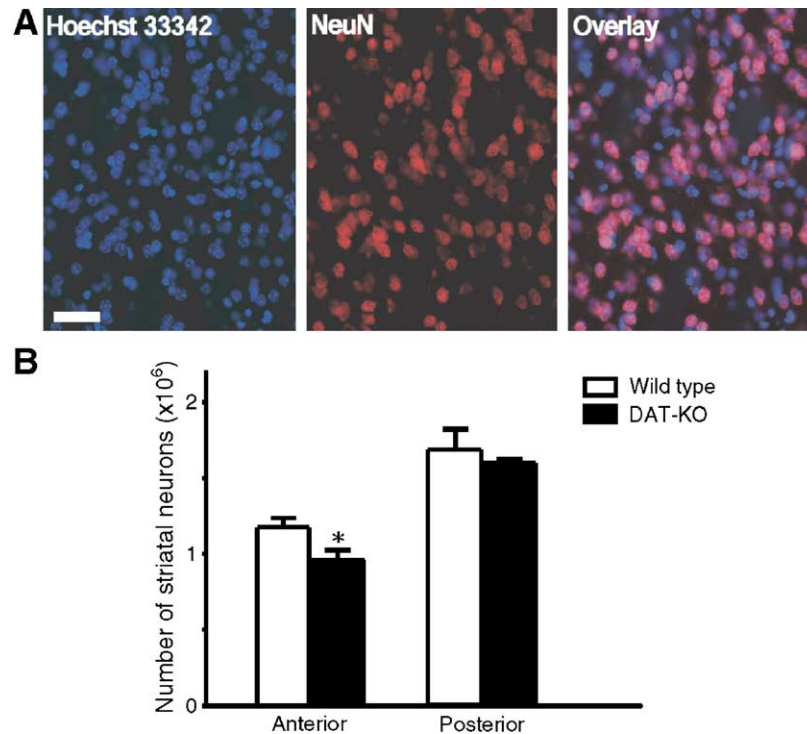


Fig. 5. Histological studies revealed the absolute number of neuronal cells. (A) Immunofluorescence analysis in which striatal cells are stained using Hoechst dye 33342 (blue) and striatal neurons by using NeuN antibody (red). Neuronal cells are positive for Hoechst dye 33342 and NeuN antibody at the same time (see overlay, pink). (B) Strict stereological method revealed the absolute number of neurons calculated in the anterior and posterior part of striatum in wild type and dopamine transporter knockout (DAT-KO) mice. Data are the average neuronal counts  $\pm$ SEM of 4 mice/group. \* $P < 0.05$  WT vs. DAT-KO mice based on Student's two-tailed  $t$  test.

(Abi-Dargham et al., 2000; Carlsson et al., 2000; Castellanos and Tannock, 2002; Gogtay et al., 2002; Gur et al., 1998; Hietala et al., 1995; Keshavan et al., 1998; Peterson et al., 2003; Robertson and Stern, 1997; Shenton et al., 2001; Swanson and Volkow, 2002; Tamminga and Carlsson, 2002). In humans, the caudate nucleus functionally corresponds to the anterior striatum in mice and both structures are related to emotion and cognition in the brain (Phillips et al., 2003). Therefore, the volumetric MRI measurements in DAT-KO mice, that exhibit also an increased DA neurotransmission, parallel the human findings. In that sense, our results suggest that increased dopaminergic tone may underlie some of the morphological and cellular brain abnormalities observed in neuropsychiatric disorders. In addition, this study in the DAT-KO mice documents the identification of factors influencing the changes in the volume of structures, which are difficult and even impossible to identify in humans with various neurological and psychiatric conditions (Weinberger and McClure, 2002). Therefore, our data also suggest that connecting MRI studies and their corresponding histopathological changes in genetically altered mouse models could be informative toward a better understanding of the clinical significance of brain MRI studies in human diseases.

#### Acknowledgments

We are grateful to B. Fubara, W.C. Kurylo, and Dr. L. Hedlund for excellent technical assistance. We also thank R.R. Gainetdinov, S. Marion, and M.A. Prado for critical comments on the manuscript. This work was supported in part by grants from NIH NS19576 and DA13511 (to M.G.C.) and NIH/NCRP (P41 05959)

(to G.A.J.). M.C. is the recipient of Huntington's Disease Society of America fellowship. A.L. was partially supported by the Academy of Finland.

#### Appendix A. Supplementary data

Supplementary data associated with this article can be found, in the online version, at [doi:10.1016/j.neuroimage.2005.01.039](https://doi.org/10.1016/j.neuroimage.2005.01.039).

#### References

- Abi-Dargham, A., Rodenhiser, J., Printz, D., Zea-Ponce, Y., Gil, R., Kegeles, L.S., Weiss, R., Cooper, T.B., Mann, J.J., Van Heertum, R.L., Gorman, J.M., Laruelle, M., 2000. Increased baseline occupancy of D2 receptors by dopamine in schizophrenia. *Proc. Natl. Acad. Sci. U. S. A.* 97, 8104–8109.
- Benveniste, H., Kim, K., Zhang, L., Johnson, G.A., 2000. Magnetic resonance microscopy of the C57BL mouse brain. *NeuroImage* 11, 601–611.
- Carlsson, A., Waters, N., Waters, S., Carlsson, M.L., 2000. Network interactions in schizophrenia-therapeutic implications. *Brain Res. Brain Res. Rev.* 31, 342–349.
- Castellanos, F.X., Tannock, R., 2002. Neuroscience of attention-deficit/hyperactivity disorder: the search for endophenotypes. *Nat. Rev., Neurosci.* 3, 617–628.
- Cyr, M., Beaulieu, J.M., Laakso, A., Sotnikova, T.D., Yao, W.D., Bohn, L.M., Gainetdinov, R.R., Caron, M.G., 2003. Sustained elevation of extracellular dopamine causes motor dysfunction and selective degeneration of striatal GABAergic neurons. *Proc. Natl. Acad. Sci. U. S. A.* 100, 11035–11040.

- Fernagut, P.O., Diguët, E., Jaber, M., Bioulac, B., Tison, F., 2002. Dopamine transporter knock-out mice are hypersensitive to 3-nitropropionic acid-induced striatal damage. *Eur. J. Neurosci.* 15, 2053–2056.
- Fernagut, P.O., Chalon, S., Diguët, E., Guilloteau, D., Tison, F., Jaber, M., 2003. Motor behaviour deficits and their histopathological and functional correlates in the nigrostriatal system of dopamine transporter knockout mice. *Neuroscience* 116, 1123–1130.
- Gainetdinov, R.R., Wetsel, W.C., Jones, S.R., Levin, E.D., Jaber, M., Caron, M.G., 1999. Role of serotonin in the paradoxical calming effect of psychostimulants on hyperactivity. *Science* 283, 397–401.
- Gainetdinov, R.R., Mohn, A.R., Caron, M.G., 2001. Genetic animal models: focus on schizophrenia. *Trends Neurosci.* 24, 527–533.
- Giros, B., Jaber, M., Jones, S.R., Wightman, R.M., Caron, M.G., 1996. Hyperlocomotion and indifference to cocaine and amphetamine in mice lacking the dopamine transporter. *Nature* 379, 606–612.
- Gogtay, N., Giedd, J., Rapoport, J.L., 2002. Brain development in healthy, hyperactive, and psychotic children. *Arch. Neurol.* 59, 1244–1248.
- Gur, R.E., Maany, V., Mozley, P.D., Swanson, C., Bilker, W., Gur, R.C., 1998. Subcortical MRI volumes in neuroleptic-naïve and treated patients with schizophrenia. *Am. J. Psychiatry* 155, 1711–1717.
- Hietala, J., Syvalahti, E., Vuorio, K., Rakkolainen, V., Bergman, J., Haaparanta, M., Solin, O., Kuoppamäki, M., Kirvelä, O., Ruotsalainen, U., et al., 1995. Presynaptic dopamine function in striatum of neuroleptic-naïve schizophrenic patients. *Lancet* 346, 1130–1131.
- Jaber, M., Dumartin, B., Sagne, C., Haycock, J.W., Roubert, C., Giros, B., Bloch, B., Caron, M.G., 1999. Differential regulation of tyrosine hydroxylase in the basal ganglia of mice lacking the dopamine transporter. *Eur. J. Neurosci.* 11, 3499–3511.
- Johnson, G.A., Benveniste, H., Black, R.D., Hedlund, L.W., Maronpot, R.R., Smith, B.R., 1993. Histology by magnetic resonance microscopy. *Magn. Reson. Q.* 9, 1–30.
- Johnson, G.A., Cofer, G.P., Fubara, B., Gewalt, S.L., Hedlund, L.W., Maronpot, R.R., 2002. Magnetic resonance histology for structural phenotyping. *J. Magn. Reson. Imaging* 16, 423–429.
- Jones, S.R., Gainetdinov, R.R., Jaber, M., Giros, B., Wightman, R.M., Caron, M.G., 1998. Profound neuronal plasticity in response to inactivation of the dopamine transporter. *Proc. Natl. Acad. Sci. U. S. A.* 95, 4029–4034.
- Keshavan, M.S., Rosenberg, D., Sweeney, J.A., Pettegrew, J.W., 1998. Decreased caudate volume in neuroleptic-naïve psychotic patients. *Am. J. Psychiatry* 155, 774–778.
- Oorschot, D.E., 1996. The total number of neurons in the neostriatum, pallidal, subthalamic and substantia nigral nuclei of the rat basal ganglia: a stereological study using the Cavalieri and optical disector method. *J. Comp. Neurol.* 366, 580–599.
- Pakkenberg, B., Gundersen, H.J., 1997. Neocortical neuron number in humans: effect of sex and age. *J. Comp. Neurol.* 384, 312–320.
- Paxinos, G., Franklin, K.J., 2001. *The Mouse Brain in Stereotaxic Coordinates*. Academic, San Diego.
- Peterson, B.S., Thomas, P., Kane, M.J., Scahill, L., Zhang, H., Bronen, R., King, R.A., Leckman, J.F., Staib, L., 2003. Basal ganglia volumes in patients with Gilles de la Tourette syndrome. *Arch. Gen. Psychiatry* 60, 415–424.
- Phillips, M.L., Drevets, W.C., Rauch, S.L., Lane, R., 2003. Neurobiology of emotion perception II: implications for major psychiatric disorders. *Biol. Psychiatry* 54, 515–528.
- Redwine, J.M., Kosofsky, B., Jacobs, R.E., Games, D., Reilly, J.F., Morrison, J.H., Young, W.G., Bloom, F.E., 2003. Dentate gyrus volume is reduced before onset of plaque formation in PDAPP mice: a magnetic resonance microscopy and stereologic analysis. *Proc. Natl. Acad. Sci. U. S. A.* 100, 1381–1386.
- Robertson, M.M., Stern, J.S., 1997. The Gilles de la Tourette syndrome. *Crit. Rev. Neurobiol.* 11, 1–19.
- Shenton, M.E., Dickey, C.C., Frumin, M., McCarley, R.W., 2001. A review of MRI findings in schizophrenia. *Schizophr. Res.* 49, 1–52.
- Sotelo, C., 1975. Anatomical, physiological and biochemical studies of the cerebellum from mutant mice: II. Morphological study of cerebellar cortical neurons and circuits in the weaver mouse. *Brain Res.* 94, 19–44.
- Swanson, J.M., Volkow, N.D., 2002. Pharmacokinetic and pharmacodynamic properties of stimulants: implications for the design of new treatments for ADHD. *Behav. Brain Res.* 130, 73–78.
- Tamminga, C.A., Carlsson, A., 2002. Partial dopamine agonists and dopaminergic stabilizers, in the treatment of psychosis. *Curr. Drug Targets. CNS Neurol. Disord.* 1, 141–147.
- Weinberger, D.R., McClure, R.K., 2002. Neurotoxicity, neuroplasticity, and magnetic resonance imaging morphometry: what is happening in the schizophrenic brain? *Arch. Gen. Psychiatry* 59, 553–558.
- Yao, W.D., Gainetdinov, R.R., Arbuckle, M.I., Sotnikova, T.D., Cyr, M., Beaulieu, J.M., Torres, G.E., Grant, S.G., Caron, M.G., 2004. Identification of PSD-95 as a regulator of dopamine-mediated synaptic and behavioral plasticity. *Neuron* 41, 625–638.